Smart Materials and Structures

PAPER • **OPEN ACCESS**

Active stiffness tuning of lattice metamaterials

To cite this article: Parham Mostofizadeh *et al* 2024 *Smart Mater. Struct.* **33** 065001

OPEN ACCESS
IOP Publishing
Smart Materials and Structures
Smart Mater. Struct. **33** (2024) 065001 (12pp)
https://doi.org/10.1088/1361-665X/ad40e7

Active stiffness tuning of lattice metamaterials

Parham Mostofizadeh, Robert A Dorey and Iman Mohagheghian*

School of Mechanical Engineering Sciences, University of Surrey, Guildford GU2 7XH, United Kingdom

E-mail: i.mohagheghian@surrey.ac.uk

Received 4 January 2024, revised 22 February 2024
Accepted for publication 19 April 2024
Published 3 May 2024

Abstract

In this paper, surface conductive heating was utilized to actively control the stiffness of lattice metamaterials manufactured employing multi-material 3D printing. To create an electrical surface conduction, additively manufactured samples in single and dual material configurations were dip coated in a solution of carbon black in water. Electro-thermo-mechanical tests conducted successfully demonstrated that the low-cost conductive coating can be used to actively alter the stiffness of the structure through surface joule heating. The process was found to result in repeatable and reproduceable stiffness tuning. Stiffness reductions of 56% and 94% were demonstrated for single and dual material configurations under the same electrical loading. The proposed methodology can be implemented to actively control the properties of polymeric lattice materials/structures where the change in the composition of polymers (introduce bulk electrical conductivity) is difficult and can have a wide range of applications in soft robotics, shape-changing, and deployable structures.

Keywords: active structures, variable stiffness structures, lattice metamaterials, conductive coating

1. Introduction

In the quest for the ultimate lightweight and high-strength material, investigations have turned to mechanical metamaterials. Purposefully-introduced porosity emerges as a promising route to reduce weight, but also to create unique properties not found in natural materials [1]. As a result, researchers are increasingly channeling their efforts into meticulously crafting architectured materials that defy the limits of traditional bulk materials. Moreover, in pursuit of enhanced weight reduction of different devices, there is a mounting motivation to engineer multifunctional metamaterials that can concurrently fulfill several objectives. A self-aware implant capable of observing the healing process of human's bone [2], a thermally-activated multi-material structure whose snapping sequence can be altered by using temperature variations [3], and a hydro-responsive metamaterial with adjustable stress–strain response [4] are amongst the examples in this regard.

Lattice metamaterials, characterized by their predetermined unit cells, represent a focal area of research exploration, renowned for their exceptional efficiency considering their weight [5]. Inspired by nature, facilitated by advanced 3D printing technologies and, more recently, accelerated by machine learning (ML) techniques, design and manufacture of these materials have garnered increasing attention [5]. In addition to their interesting mechanical properties, it has always been desirable to embed multiple functionalities into lattice materials, thereby enhancing their overall capabilities and performance. Noteworthy endeavors in this direction encompass the fabrication of 3D-printed multi-material cellular materials that leverage buckling phenomena for tunable actuation force [6], a multifunctional cross-flow heat exchanger based on a hollow lattice design endowed with mechanical load bearing capability [7], and the design of a 3D impedance-type lattice structure capable of absorbing broadband radar frequencies while simultaneously withstanding out-of-plane loads [8].

* Author to whom any correspondence should be addressed.

To further improve the functionality of these materials, it is imperative to transition towards active materials capable of responding to the varying ambient situations. Such a shift can have great implications in cost and weight saving, particularly in scenarios characterized by a lot of constraints, such as space structures [9]. For instance, the thermally-activated lattice structure conceptualized by Wagner *et al* [9] is capable of switching topology and, as a result, moving between bending- and stretching-dominated modes which demonstrate different mechanical responses. Lumpe and Shea [10] utilized multi-material 3D printing method to fabricate active lattice structures that are capable of reversible shape morphing when exposed to heat and can be exploited as an airfoil. Hoh *et al* [11] designed a 3D electro-lattice actuator that, when actuated by an electrical current, can transform into a thin sheet. The spring-like characteristics of the suggested actuator render it well-suited for implementation in modules that require variable stiffness. Dudek *et al* [12] introduced novel 3D metamaterials featuring magnetic inclusions, showcasing a tunable range of negative stiffness values from -5 kN m^{-1} to 0. Additionally, their study revealed that altering the orientation of the magnets within the material could lead to either negative or positive stiffness in the structure. Similarly, Galea *et al* [13] devised an innovative accordion-like metamaterial capable of undergoing recoverable dimensional variations. Upon exposure to a magnetic stimulus, the design metamaterial could exhibit a switch in its Poisson's ratio from negative to positive.

In the forthcoming sections of this research paper, we endeavor to elucidate the considerable promise inherent in the active stiffness tuning as an innovative avenue for enhancing the efficiency of lattice structures. Specifically, we have designed and fabricated a 2D diamond lattice structure utilizing Polyjet technology, both in single-material and multi-material configurations. Subsequently, a conductive coating has been applied to both structures, facilitating their activation through the application of electrical current. It is noteworthy that the two polymers employed in this study exhibit distinct glass transition temperatures, resulting in dissimilar thermoplastic softening behaviors when subjected to Joule heating.

2. Methods

2.1. Materials and fabrication

Single- and multi-material lattices were fabricated using a Stratasys Objet260 Connex3 3D printer (MN, USA) which works based on Polyjet technology. Two different polymers, VeroWhite and FLX9895-DM, were selected for the fabrication process due to their differing characteristics, including stiffness and glass transition temperature (T_g). To assess their behavior, Dynamic Mechanical Analysis (DMA) and compression tests were performed on samples made from these materials. The DMA tests were carried out in temperature ramp mode at a frequency of 1 Hz and a heating rate of 2 °C min^{-1}, applying a 10 μm loading amplitude, using a three-point bending clamp on the DMA Q800 machine (TA Instruments, DE, USA). The test samples were 3D printed in rectangular shapes with dimensions of 25 × 10 × 2 mm. Compression tests were performed on samples 3D printed in cylindrical shape with a diameter of 12.7 mm and a height of 25.4 mm, following the ASTM D695–15 standard, using an Instron 5500 universal machine (MA, USA) with a strain rate of 10^{-4} s^{-1}.

2.2. Coating method

The polymers utilized for the fabrication of the designed structures lack inherent electrical conductivity. In order to impart electrical conductivity to these structures, a conductive coating layer needed to be applied to the sample surfaces. Presently, there exists a variety of coating techniques, some of which are compatible with mass manufacturing procedures. Thermal Spray Coating, Spin Coating, Chemical Vapor Deposition (CVD), and Atomic Layer Deposition (ALD) are just some of the available methods. Each of these approaches possesses distinct constraints and prerequisites. Consequently, not all techniques are suitable to the polymeric lattice structures under investigation. A comparison of these methods is provided in table 1. It is imperative to acknowledge that the evaluations shown in this table are entirely qualitative in nature and do not enable direct quantitative comparisons.

In the context of lattice structures, the selection of an appropriate coating method is constrained by the intricate geometry of these structures. Additionally, considerations such as achieving uniform coating coverage on all surfaces, the deformability of the coating, and the capacity to achieve the desired temperature increase are critical when choosing the appropriate coating method. Furthermore, the specific characteristics of the materials used in this research impose limitations on the temperature levels that can be employed during the coating process, rendering high-temperature methods impractical. These influential factors collectively led to the adoption of the Dip Coating method as a viable option for the structures under investigation. This method provides a high degree of control over coating thickness, particularly when extremely thin or thick coatings are not required [19]. Moreover, it was chosen as the fastest and most efficient method amongst the available options, as it enables the efficient utilization of the prepared solution without waste [19]. To ensure uniformity and repeatability in coating thickness, the dipping speed was carefully regulated using a motorized crane with a constant head speed of 20 cm min^{-1} .

2.3. Coating solution

The chosen coating methodology, aimed at achieving a cost-effective and energy-efficient approach for applying a conductive coating to the investigated materials, led to the selection of *carbon black* as the preferred coating material. To prepare the coating solution, carbon black, acetylene, 50% compressed with a density of 1.95 g cm^{-3} purchased from Alfa Aesar was dissolved in pure water. Polyvinyl alcohol (PVA) was added as the binder. PVA was purchased from Aldrich

Table 1. Comparison between some conventional coating methods (higher rating corresponding to better capability).

Method	Speed	Operating Temperature	Capability of Dealing with Complex Geometries	Ease of Use
Thermal Spray Coating [14–16]	★★	Low-High	★★	★
Spin Coating [17, 18]	★★★	Low	★	★★
Dip Coating [19, 20]	★	Low	★★★	★★★
Atomic Layer Deposition [21, 22]	★	Low-Medium	★★★	★
Chemical Vapor Deposition [23, 24]	★★	Low-High	★★★	★

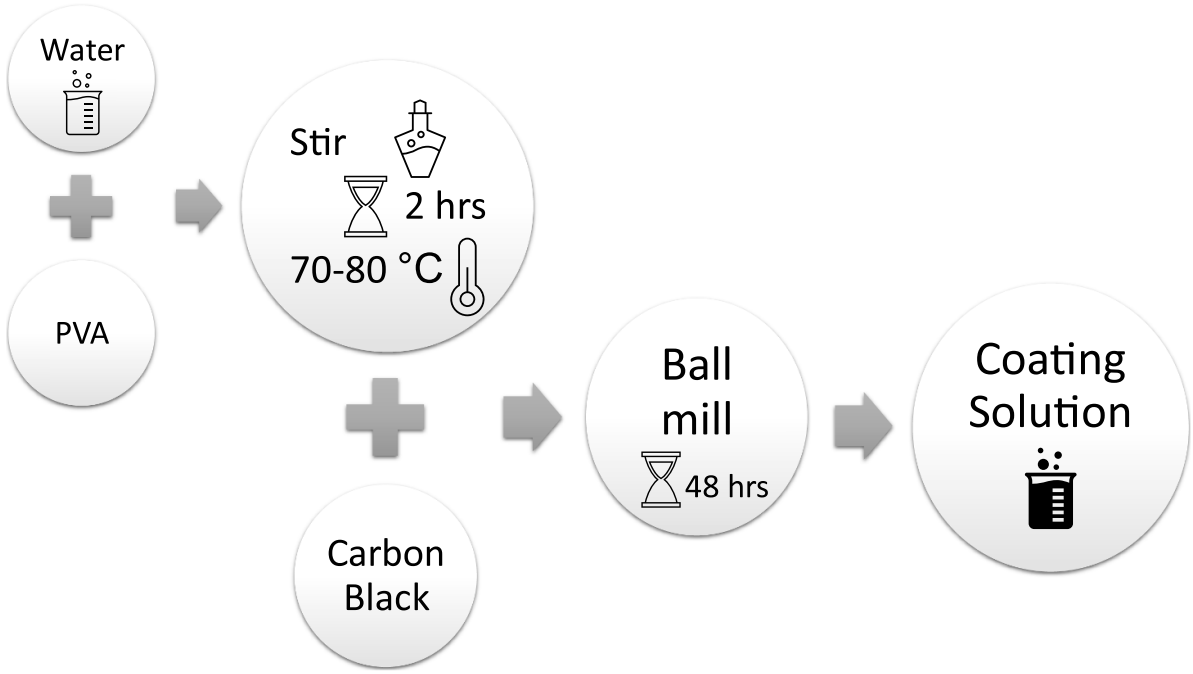

Figure 1. Coating solution preparation process.

which had a density of 1.25 g cm^{-3} and its volumetric ratio to carbon black was maintained at 20%. The preparation procedure involved dissolving PVA in an appropriate volume of pure water through stirring at temperatures ranging from 70 to 80 °C for a duration of 2 h. Subsequently, carbon black was incorporated into the solutions and subjected to 48 h of ball milling. Figure 1 illustrates the process of solution preparation.

Initially, 1, 2, and 3 volumetric percent solutions of carbon to water were prepared. These solutions were subsequently applied to rectangular samples, each measuring 20 × 8 × 2 mm, which were fabricated using FLX9895-DM with a matte finish via 3D printing. Before dipping the samples, the solution was put into an ultrasonic bath of water at room temperature for 20 min. To assess the suitability of each solution, five distinct dipping trials were conducted on five separate samples for each volumetric percentage. The electrical resistance between the two longer edges of the samples was measured to determine the optimal solution. Based on the resistance results, the 2% concentration solution was selected, as no significant improvement in electrical conductivity was observed when the concentration was increased to 3%.

2.4. Application of the coating to lattices

The 2 wt% carbon solution was employed for the surface coating of single and multi-material 2D modified-diamond lattice structures containing an additional horizontal strut. By introducing a multi-material design, the horizontal strut facilitates enhanced manipulation of node connectivity and improved control over mechanical behavior. In these lattices, VeroWhite and FLX9895-DM sections were 3D printed with glossy and matte finishes, respectively. The single-material lattice was entirely manufactured using FLX9895-DM, whereas VeroWhite was exclusively employed to build the frame areas of the multi-material lattice, as depicted in figure 2(a). Figure 2(b) demonstrates the direction according to which each sample was dipped inside the solution. To create similar potential across, the two front and rear surfaces were covered with silver paint (Electrodag 1415, Agar Scientific). Subsequently, the resistance of the coated samples was quantified using a Keithley 2110 multimeter with an accuracy of 0.020% [25]. In the case of these lattice structures, it was determined that a three-round immersion in the solution sufficiently enhanced resistance in the direction of the lattices'

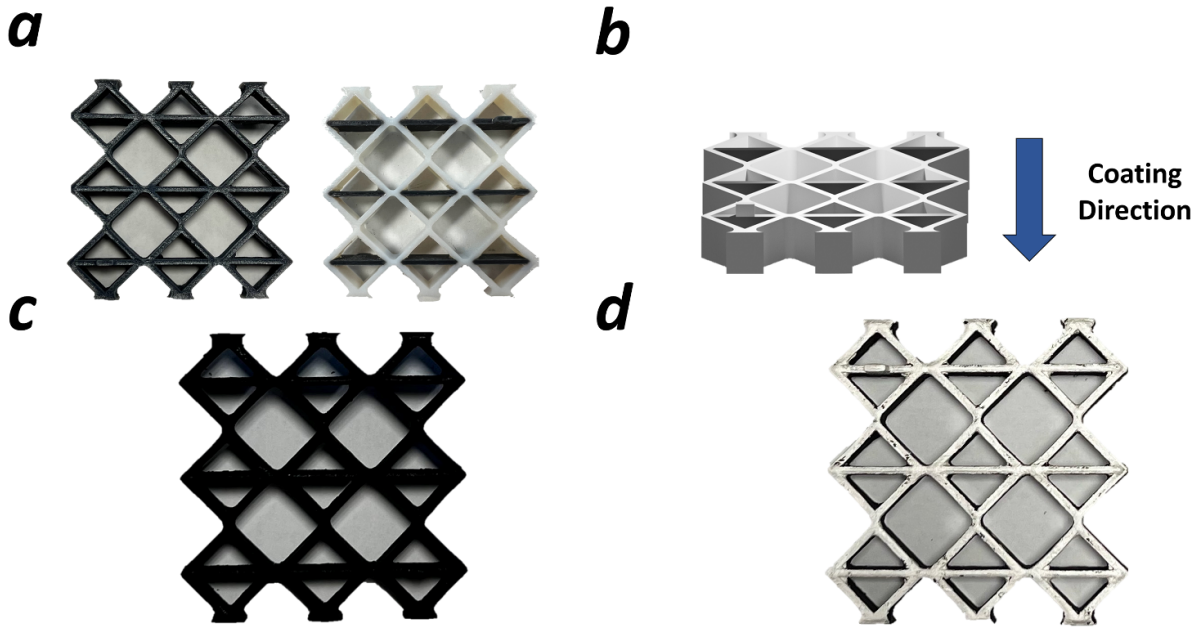

Figure 2. Coating process of the 2D diamond lattice single- (FLX9895-DM) and multi-material (VeroWhite and FLX9895-DM) (a) lattices as manufactured (b) direction of carbon-coating (c) carbon-coated lattice (d) lattice after applying silver paint.

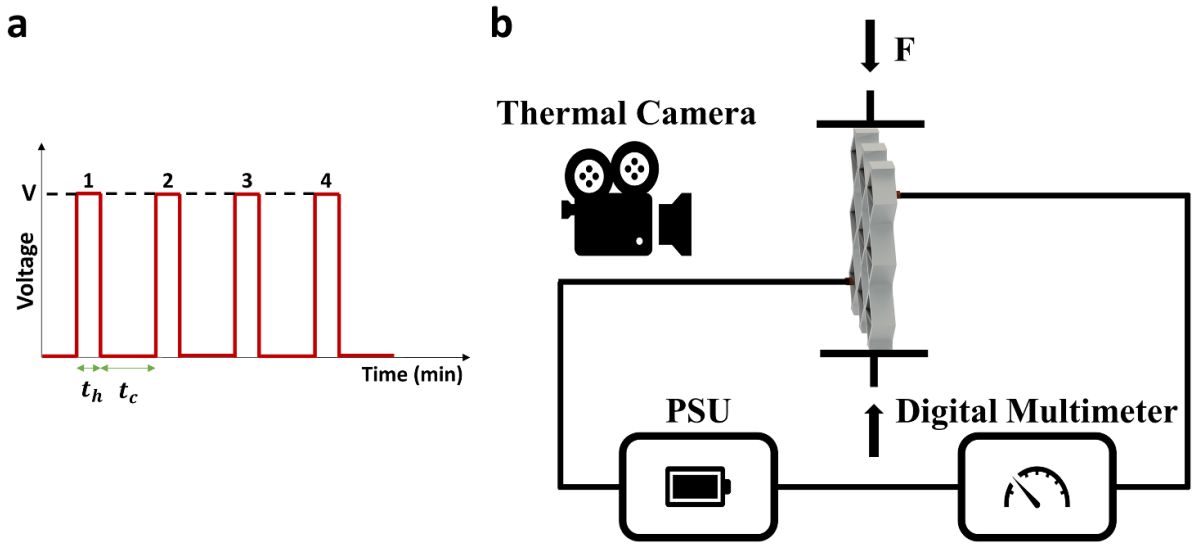

Figure 3. (a) Schematic of the electrical cycles applied to the coated samples (b) the setup used for the electro-mechanical tests on the coated 2D diamond samples.

extrusion orientation, which corresponds to the direction of the coating.

2.5. Electro-thermo-mechanical testing of coated lattice structures

In order to investigate the thermal behavior of the coating, a 'top-hat' cyclic electrical load, as depicted in figure 3(a) (with t_h representing heating time and t_c representing cooling time, each lasting 2.5 min), was applied to the samples using a maximum voltage of 12 V. The temperature of the lattice was monitored using a FLIR A6751 thermal imaging camera with an accuracy of ±2 °C [26]. The camera's measurements underwent calibration by using a black plate and setting the emissivity to 0.95. It is worth noting that the implementation of a high emissivity carbon-based coating on the structures minimized potential reflections from external thermal emissions. To facilitate the connection of the samples to the power supply, two additional tabs were integrated during the 3D printing process, as shown in figure 3(b), providing a sufficient grip area for wire connections. To assess the uniformity of the coating on the sample's surface, a cross-sectional sample was embedded in epoxy and polished until a clear surface was achieved. The coating's consistency at various locations on the sample was examined using a KEYENCE VHX-7000 digital microscope.

Prior to subjecting the samples to electrical loading, cyclic compression tests with increasing strain amplitudes were carried out on a coated single-material sample, while monitoring its resistance. This was done to determine the maximum strain the coating could withstand without altering its behavior. The results from these compression tests were employed as a reference in subsequent electro-thermo-mechanical tests.

To assess the effectiveness of the joule heating of the conductive coating in decreasing the mechanical properties of the lattice structures, compression tests were conducted while the sample was under electrical loading. For the electro-mechanical experiments, samples were subjected to compression at a strain rate of 10^{-4} s^{-1} under two distinct conditions: without the application of electrical current and with electrical current applied. Prior to imposing the mechanical loading, a voltage of 12 V was applied to the samples for one minute to elevate their temperature from the initial ambient temperature which was recorded to be 24 °C at the time of the tests. Throughout the testing process, the temperature of the samples was continuously monitored using the thermal camera. Figure 3(b) demonstrates the experimental setup employed for these tests.

3. Results and discussion

3.1. 3D printing material properties

Figure 4 depicts the DMA and compression test results of the two materials used in this study. The glass transition temperatures of VeroWhite and FLX9895-DM were determined to be 66.5 °C and 23.0 °C, respectively, based on the peak of the Tan δ curve. Additionally, the elastic modulus of VeroWhite and FLX9895-DM was obtained by fitting a line to the stress–strain curves within the strain range of 0.8%–1%, yielding values of 2555.0 MPa and 15.9 MPa, respectively.

3.2. Study of coating on the single- and multi-material lattices

The electrical resistances of the carbon coated single- and multi-material 2D diamond samples, measured along their thickness, are listed in table 2. For each configuration, the average resistance of the three tested specimens is also shown.

The results demonstrate good consistency among the samples in each category, indicative of the repeatability of the coating technique. As evident from table 2, multi-material samples exhibit higher conductivity when compared to their single-material counterparts. Specifically, the former shows 37% less resistance than the latter. To further investigate this disparity, the lattice cross-sections (figure 5(a)) were examined to assess the coating layers in different regions of the figure 5(s)ingle-material and multi-material samples using an optical microscope, as shown in figures 5(b) and (c), respectively.

By comparing figures 5(b) and (c), minimal differentiation is observed in the coating of the central struts, as both cases involve struts fabricated from identical materials with similar surface finishing. However, a notable disparity arises between the two values with respect to the thickness of the coating deposited on the frame. In the latter scenario, the frame areas are produced using VeroWhite with a glossy finish, leading to a reduced carbon deposition on their surfaces. Even though the coating is thinner on the VeroWhite sections of the multi material system the overall electrical resistance is lower as table 2 the presence of cracks or gaps in the coating on the matte surface of FLX9895-DM have a more detrimental effect.

3.3. Electro-thermal response of the coated lattice structures

By subjecting the specimens to a cyclic electrical current, as illustrated in figure 3(a), and monitoring the surface temperature at the end of each cycle, the thermal profiles presented in figures 6 and 7 were derived.

In order to quantitatively examine the results shown in figures 6 and 7, the average surface temperature of the visible through-thickness walls (gray surfaces in figure 8) was calculated and is shown in figure 8(a) at the end of each heating and cooling cycle. Furthermore, figures 8(b) and (c) depict the variations in the mean, maximum, and minimum temperatures of a representative sample across four cycles, both for single-material and multi-material specimens. Through a comparative analysis of the outcomes depicted in figure 6 for single-material samples and figure 7 for multi-material samples, it becomes evident that the latter exhibits a greater variation in stiffness after actuation. This, coupled with the noticeable increase in difference between the mean, maximum, and minimum temperatures of the multi-material sample compared to the single-material counterpart, as depicted in figures 8(a) and (c), and film continuity from optical micrographs, highlights the effects of changes in hot spot occurrence.

The findings indicate that following three successive dipping cycles, both single- and multi-material structures acquire the capacity to generate a temperature increase of approximately 50 °C when subjected to a 12 V voltage. Additionally, the coatings on the lattice structures exhibit robust durability throughout repeated electrical loading cycles, demonstrating a repeatable behavior after three cycles. The observed behavior may potentially be ascribed to thermal buildup that has occurred within the specimens subsequent to the application of multiple heating cycles. The duration of the cooldown period proves insufficient for the sample to attain its initial state temperature (denoted by 'IS' in figure 8(a)). Nevertheless, analysis of the presented figure reveals that the sample repeatedly cools to a consistent lower temperature following the third cycle of cooldown.

3.4. Electro-mechanical response of the coated lattice structures

As previously indicated, a series of cyclic strain ramp tests were conducted to determine the maximum strain tolerance of coated structures while minimizing coating damage. The

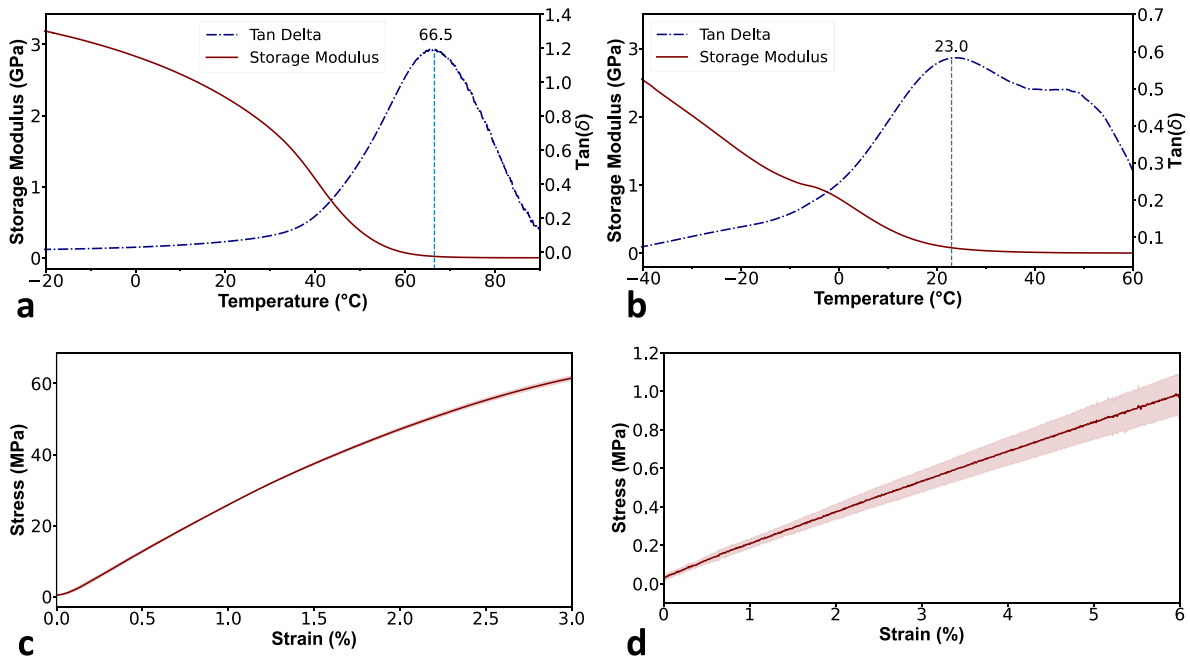

Figure 4. Mechanical characteristics of the polymers utilized for manufacturing the lattices (a) DMA plot of VeroWhite (b) DMA plot of FLX9895-DM (c) stress–strain curve of VeroWhite at 27 °C and the strain rate of 10^{-4} s^{-1} (d) stress–strain curve of FLX9895-DM at 27 °C and the strain rate of 10^{-4} s^{-1}.

Table 2. Measured resistance of the coated single- and multi-material 2D diamond lattice structures.

	Resistance (Ω)	
Sample	Single-material	Multi-material
1	33.4	23.2
2	32.0	19.0
3	30.6	18.5
Average	32.0	20.2

stress–strain response of the sample throughout five compression loading-unloading cycles with a maximum displacement of 2 mm is depicted in figure 9(a) while figure 9(b) presents the variations in the sample's resistance during a single loading and unloading cycle. Notably, due to some plastic deformation, the strain does not return to zero at the conclusion of each cycle, as depicted in figure 9(b). By subjecting the sample to five loading-unloading cycles with maximum displacements of 1 mm, 2 mm, and 5 mm, while simultaneously monitoring changes in resistance, the results shown in figures 9(c) and (d) were obtained. These figures display the resistance values at the beginning and end of each loading stage, respectively.

The data presented in these figures reveals that the sample and the applied coating exhibit minimal changes in electrical conductivity when subjected to a maximum displacement of 1 mm (corresponding to a nominal strain of 1.4%) during each loading-unloading cycle. In contrast, a maximum displacement of 5 mm, equivalent to a nominal strain of 5.4%, leads to substantial alterations in the sample's resistance. Consequently, based on these findings, a maximum displacement of 1 mm was selected for the electro-thermo-mechanical tests conducted on the coated single- and multi-material lattices.

Figures 10 and 11 show the surface temperature of the coated single- and multi-material lattices, respectively, while the electrical current was applied along with mechanical loading. These results correspond to the red curves in figures 12(a) and (b). In figure 12, the average measurements of three tested samples are shown and the standard deviation is represented by the shaded areas. Specifically, figures 12(a) and (b) provide stress–strain curves for single-material samples made from FLX9895-DM and multi-material samples composed of VeroWhite and FLX9895-DM, respectively, both with and without the application of electrical current. Figures 12(c) and (d) depict the mean, maximum, and minimum temperatures observed during the application of electrical current for the two distinct material configurations.

These findings reveal a more compliant mechanical behavior of the lattice structure upon the application of a 12 V electrical load. Notably, this decrease in stiffness is more

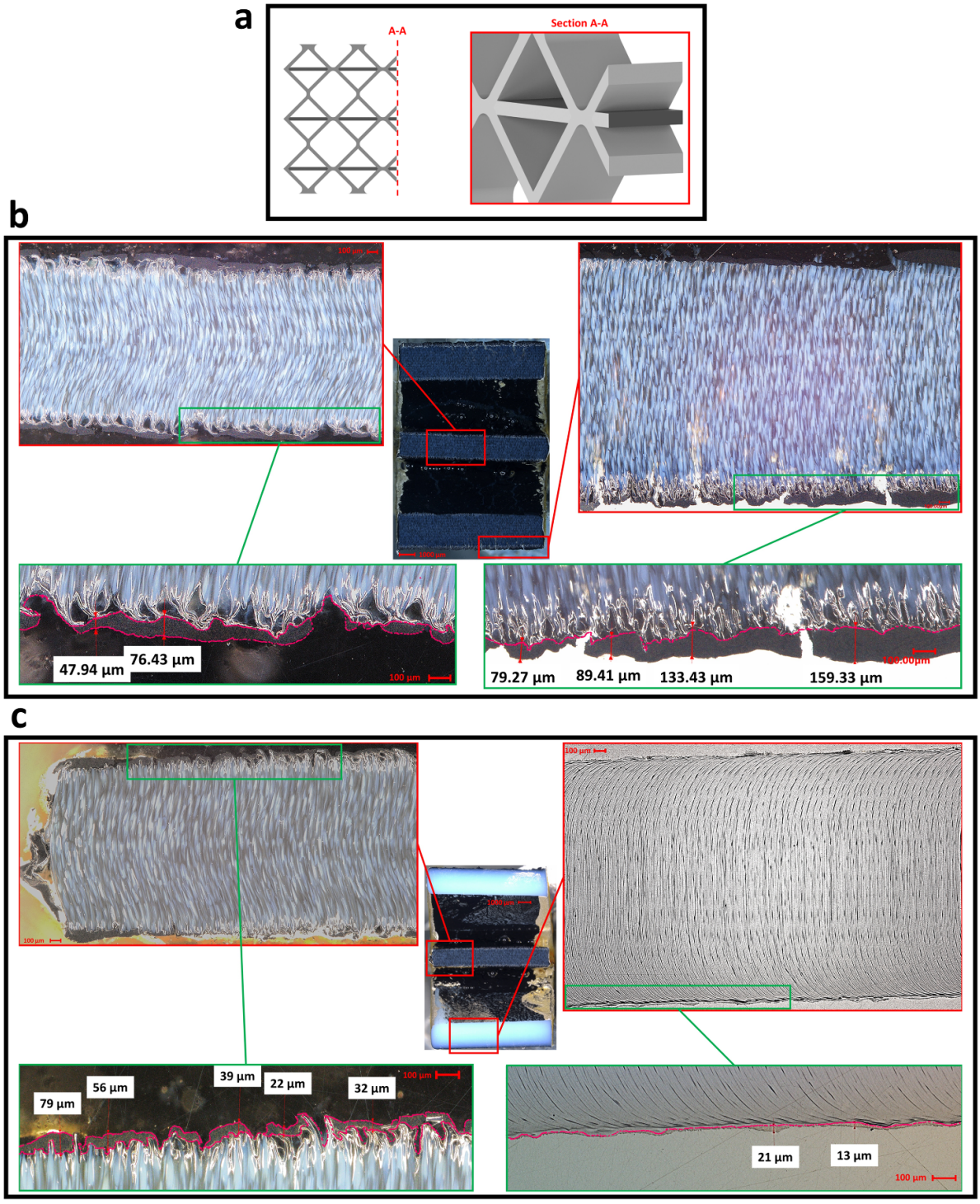

Figure 5. (a) 2D diamond lattice's cross-section used for micrographs (b) micrograph of the coated single-material and (c) multi-material 2D diamond sample alongside the detailed images of the selected areas (due to the cutting angle the thickness values shown on the bottom right should be multiplied by cos $\frac{\pi}{4}$).

pronounced in the case of the multi-material sample, as illustrated in figure 12(b). To elaborate further, for the case of single-material sample, as shown in figure 12(a), at the strain of 1.4%, the mean stress drops from 10.2 kPa to 4.5 kPa when the electrical current is applied. However, for the case of multi-material sample in figure 12(b), there is a drop from 114.9 kPa to 6.7 kPa. These values represent a reduction of approximately 56% in the single-material case and about 94% in the multi-material case. Utilizing the stress–strain curves of the multi-material sample within the strain range of

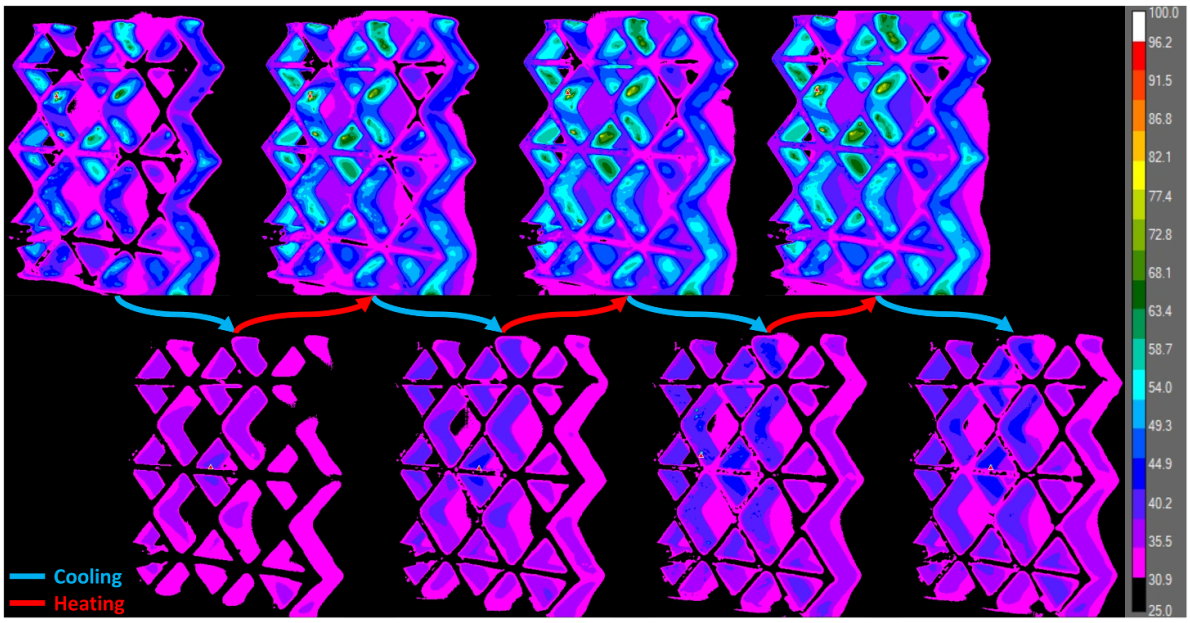

Figure 6. Thermal images of the coated single-material 2D diamond sample subjected to cyclic electrical loading. Each picture shows the thermal profile at the end of the respective heating or cooling cycle.

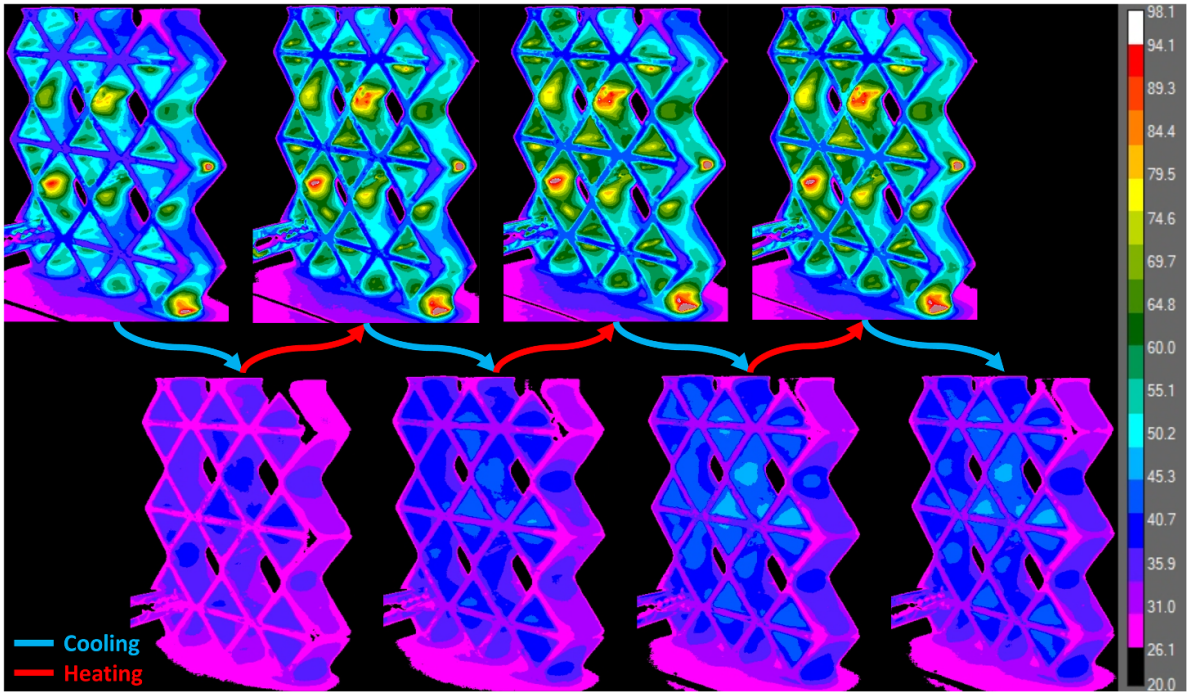

Figure 7. Thermal images of the coated multi-material 2D diamond sample subjected to cyclic electrical loading. Each picture shows the thermal profile at the end of the respective heating or cooling cycle.

0.1%–0.2%, average stiffness values of 8.0 MPa and 1.7 MPa were determined before and after thermal actuation, respectively. Comparatively, the cellular structure introduced by Wu *et al* [27] exhibits an elastic modulus of 36 kPa in the linear elastic regime, while the digital metamaterial developed by Choe *et al* [28] demonstrates a modulus of 171.2 kPa in the rigid state. These findings underscore the load-bearing capacity of the multi-material lattice proposed here, even following softening via electrical actuation. These findings emphasize the effectiveness of the conductive coating and the applied

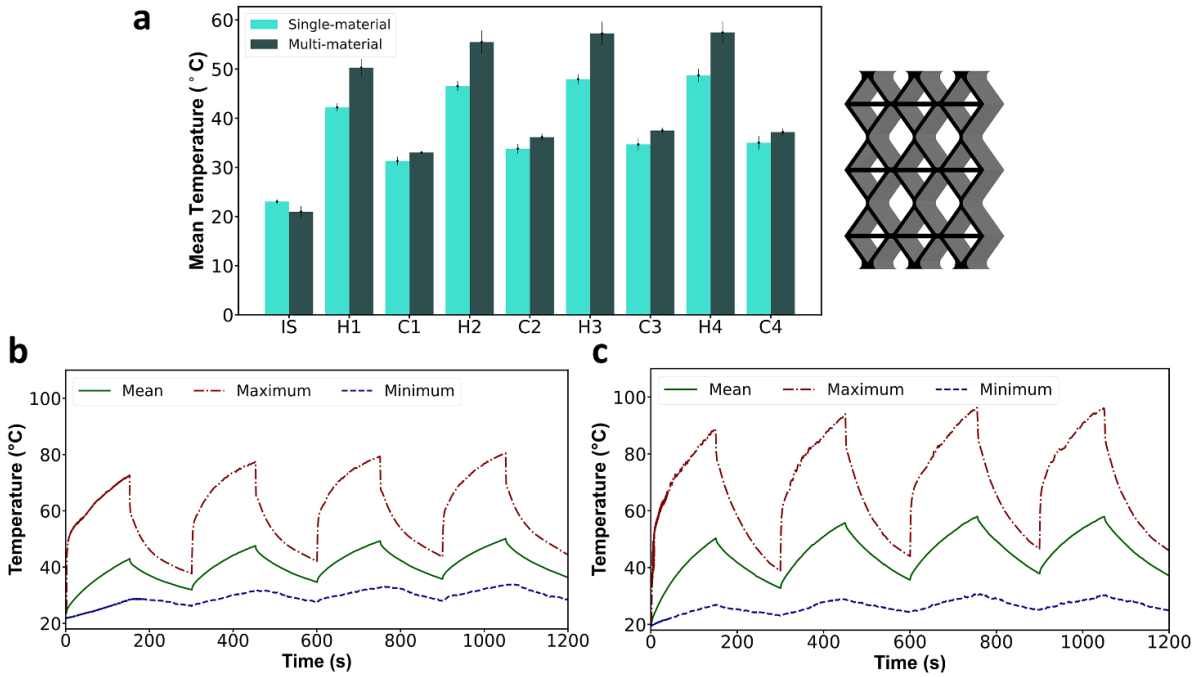

Figure 8. (a) Mean temperature of the through-thickness walls of the coated single- and multi-material 2D diamond structure during electrical cyclic loading. The gray areas demonstrate the surfaces used in thermal averaging. IS: Initial State, H: End of heating C: End of cooling down (b) variations mean, maximum, and minimum temperature of one sample versus time in the single- and (c) multi-material sample.

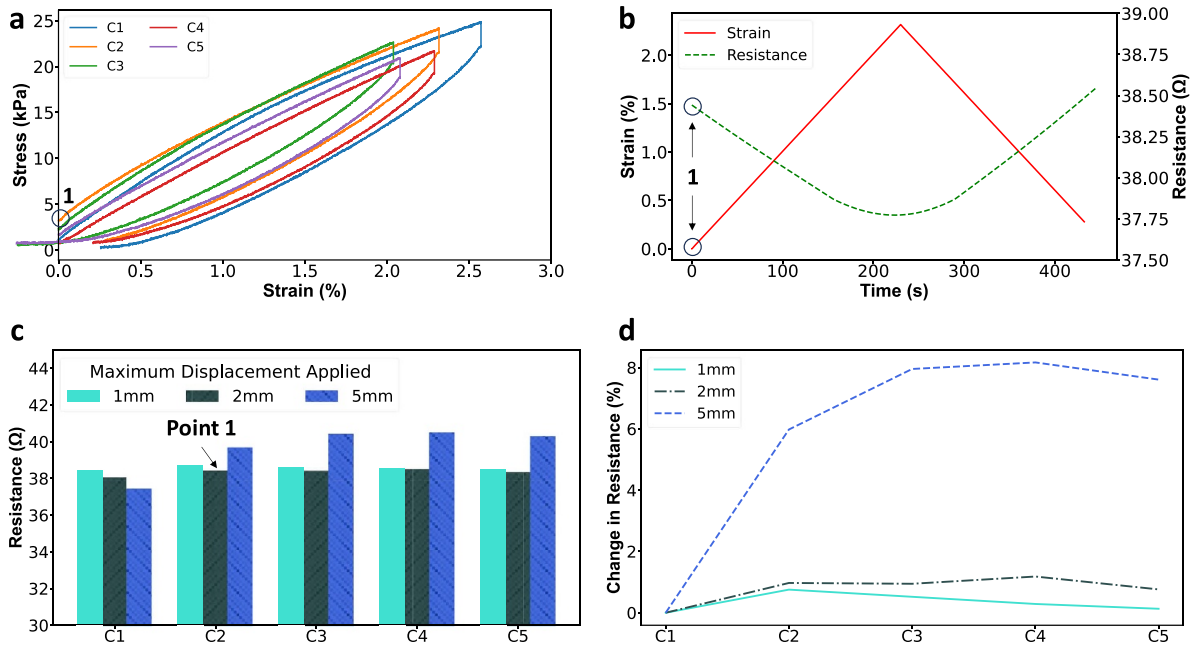

Figure 9. (a) Cyclic stress–strain plot of the coated single-material sample made from FLX9895-DM while a maximum displacement of 2 mm was applied (b) resistance variation of the sample in the second cycle (c) measured resistance of the coated single-material 2D diamond sample made from FLX9895-DM and (d) percent change in the resistance at the beginning of each loading cycle by comparing three different maximum strain applied to the sample.

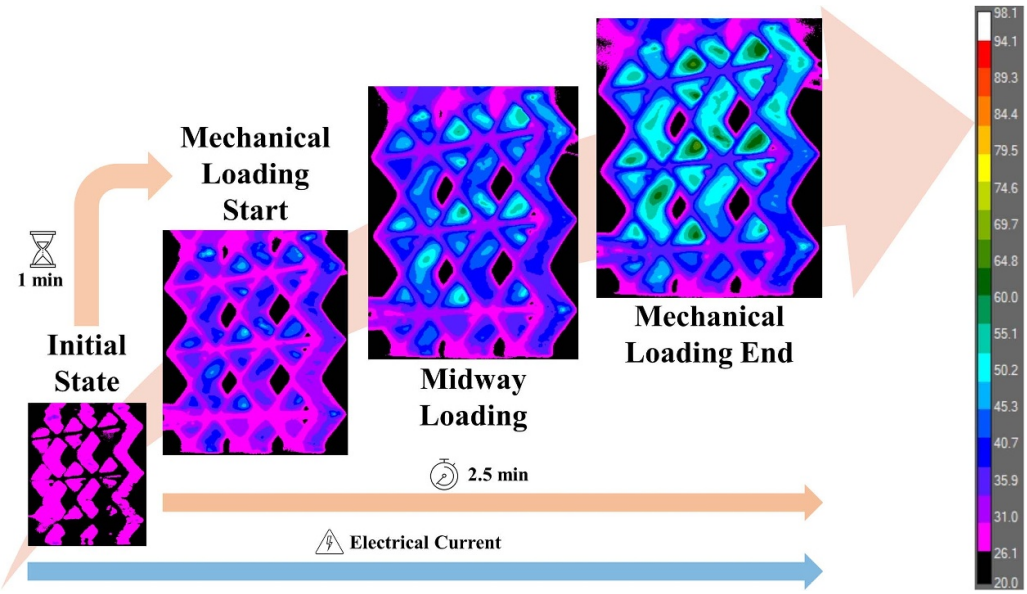

Figure 10. Temperature profile of the coated single-material 2D diamond sample under compression while exposed to Joule heating.

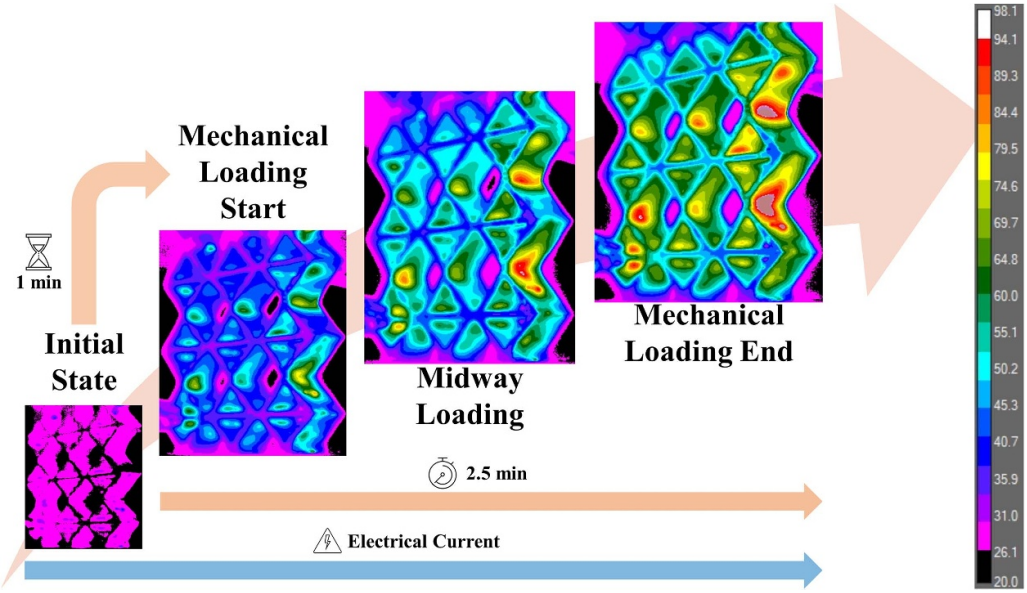

Figure 11. Temperature profile of the coated multi-material 2D diamond sample under compression while exposed to Joule heating.

technique for dynamically modulating stiffness, showcasing that dip coating, as an economical and easy-to-use process, can be employed in creating structures suitable for the active manipulation of the mechanical properties in polymer-based lattice structures. The proposed method offers a viable resolution for situations in which existing constraints prevent the incorporation of bulk electrically conductive materials. This holds significant implications across diverse applications, including but not limited to soft robotics, shape-shifting mechanisms, and deployable structures.

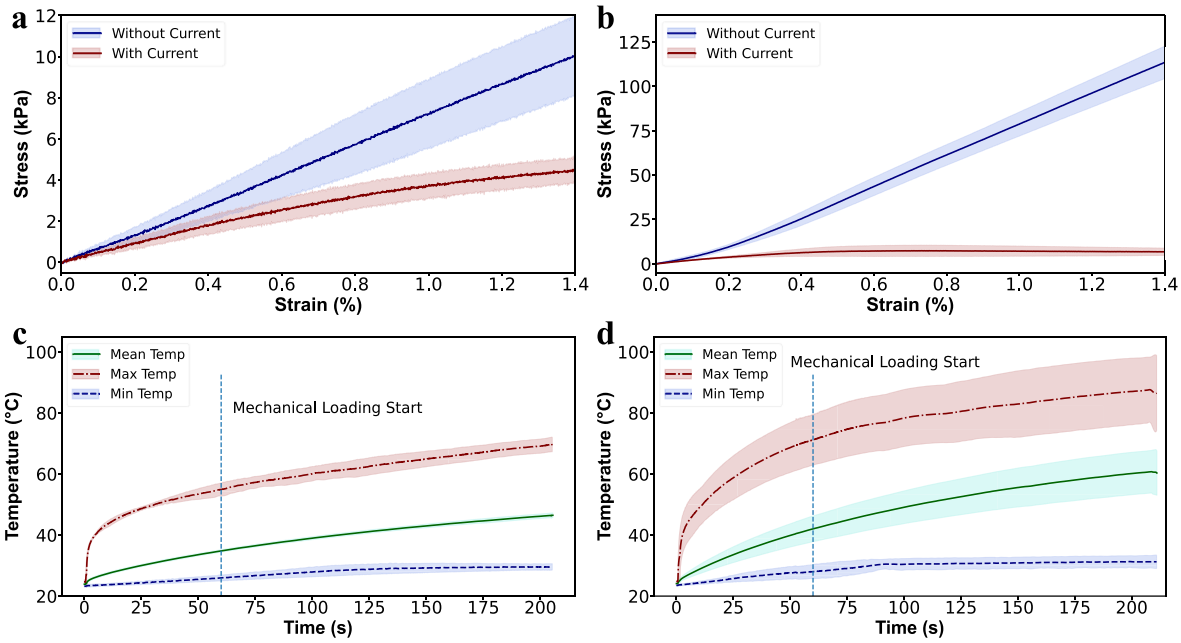

Figure 12. Stress–strain curves of the coated 2D diamond sample under compression with a maximum displacement of 1 mm with and without applying electrical load (a) single-material made from FLX9895-DM (b) multi-material made from VeroWhite and FLX9895-DM (c) variations of mean, minimum, and maximum temperatures observed in the single-material and (d) multi-material samples.

4. Concluding remarks

This research has successfully investigated the use of a low-cost conductive coating to actively control the stiffness of lattice metamaterials. It has been shown that by using a dip coating method employing a 2 volumetric percent aqueous carbon black dispersion and three rounds of immersion it is possible to achieve adequate surface electrical conductivity and the generation of sufficient heat via Joule heating to induce structural softening with a 12 V power supply. Despite the automation of the dip coating process, variations in coating thickness were observed, leading to non-uniform heating. Additionally, it was observed that the surface finish of the 3D printed part (matte vs glossy) significantly influenced the quality and consistency of the coating. Nevertheless, the study has established the repeatability and reproducibility of stiffness variations under multiple electrical loading cycles. Specifically, stiffness reductions of 56% and 94% were achieved in single and dual material configurations with similar electrical loading. This proposed methodology holds the potential to actively control the properties of polymeric lattice materials and structures, particularly in situations where altering the composition of polymers to introduce bulk electrical conductivity is challenging. The research findings have broad applications in fields such as soft robotics, shape-changing mechanisms, and deployable structures.

Data availability statement

The data that support the findings of this study are available upon reasonable request from the authors.

Acknowledgments

This work has been funded by the UK's Engineering and Physical Sciences Research Council (EPSRC, Grant reference: EP/L016788/1 and EP/T009306/1) and the University of Surrey.

Conflict of interest

The authors declare that they have no known competing financial interests or personal relationships that could have appeared to influence the work reported in this paper.

Author contributions

Parham Mostofizadeh: Formal Analysis, Investigation, Visualization, Writing—Original Draft

Robert A Dorey: Methodology, Supervision, Writing—Review & Editing

Iman Mohagheghian: Conceptualization, Methodology, Project Administration, Supervision, Validation, Writing—Review & Editing

ORCID iDs

Parham Mostofizadeh https://orcid.org/0000-0002-2598-6828
Iman Mohagheghian https://orcid.org/0000-0001-9069-0815

References

[1] Bauer J, Meza L R, Schaedler T A, Schwaiger R, Zheng X and Valdevit L 2017 Nanolattices: an emerging class of mechanical metamaterials *Adv. Mater.* **29** 1701850
[2] Barri K, Zhang Q, Swink I, Aucie Y, Holmberg K, Sauber R, Altman D T, Cheng B C, Wang Z L and Alavi A H 2022 Patient-specific self-powered metamaterial implants for detecting bone healing progress *Adv. Funct. Mater.* **32** 2203533
[3] Che K, Yuan C, Qi H J and Meaud J 2018 Viscoelastic multistable architected materials with temperature-dependent snapping sequence *Soft Matter* **14** 2492–9
[4] Zhang H, Guo X, Wu J, Fang D and Zhang Y 2018 Soft mechanical metamaterials with unusual swelling behavior and tunable stress-strain curves *Sci. Adv.* **4** eaar8535
[5] Jia Z, Liu F, Jiang X and Wang L 2020 Engineering lattice metamaterials for extreme property, programmability, and multifunctionality *J. Appl. Phys.* **127** 150901
[6] Janbaz S, Bobbert F S L, Mirzaali M J and Zadpoor A A 2019 Ultra-programmable buckling-driven soft cellular mechanisms *Mater. Horiz.* **6** 1138–47
[7] Maloney K J, Fink K D, Schaedler T A, Kolodziejska J A, Jacobsen A J and Roper C S 2012 Multifunctional heat exchangers derived from three-dimensional micro-lattice structures *Int. J. Heat Mass Transfer* **55** 2486–93
[8] Zhang Z, Lei H, Yang H, Chen M, Wang C, Yang H and Fang D 2021 Novel multifunctional lattice composite structures with superior load-bearing capacities and radar absorption characteristics *Compos. Sci. Technol.* **216** 109064
[9] Wagner M A, Lumpe T S, Chen T and Shea K 2019 Programmable, active lattice structures: unifying stretch-dominated and bending-dominated topologies *Extrem. Mech. Lett.* **29** 100461
[10] Lumpe T S and Shea K 2021 Computational design of 3D-printed active lattice structures for reversible shape morphing *J. Mater. Res.* **36** 3642–55
[11] Hoh S, Helps T, Diteesawat R S, Taghavi M and Rossiter J 2021 Electro-lattice actuator: a compliant high-contractile active lattice structure *Smart Mater. Struct.* **30** 125034
[12] Dudek K K, Gatt R and Grima J N 2020 3D composite metamaterial with magnetic inclusions exhibiting negative stiffness and auxetic behaviour *Mater. Des.* **187** 108403
[13] Galea R, Dudek K K, Farrugia P S, Zammit Mangion L, Grima J N and Gatt R 2022 Reconfigurable magneto-mechanical metamaterials guided by magnetic fields *Compos. Struct.* **280** 114921
[14] Gonzalez R, Ashrafizadeh H, Lopera A, Mertiny P and McDonald A 2016 A review of thermal spray metallization of polymer-based structures *J. Therm. Spray Technol.* **25** 897–919
[15] Kuroda S, Kawakita J, Watanabe M and Katanoda H 2008 Warm spraying—a novel coating process based on high-velocity impact of solid particles *Sci. Technol. Adv. Mater.* **9** 033002
[16] Moridi A, Hassani-Gangaraj S M, Guagliano M and Dao M 2014 Cold spray coating: review of material systems and future perspectives *Surf. Eng.* **30** 369–95
[17] Larson R G and Rehg T J 1997 Spin Coating *Liquid Film Coating: Scientific Principles and Their Technological Implications* ed S F Kistler and P M Schweizer (Springer Netherlands) pp 709–34
[18] Tyona M D 2013 A theoritical study on spin coating technique *Advances in Materials Research* vol **2** pp 195–208
[19] Grosso D 2011 How to exploit the full potential of the dip-coating process to better control film formation *J. Mater. Chem.* **21** 17033–8
[20] Dastan D, Panahi S L and Chaure N B 2016 Characterization of titania thin films grown by dip-coating technique *J. Mater. Sci., Mater. Electron.* **27** 12291–6
[21] George S M 2010 Atomic layer deposition: an overview *Chem. Rev.* **110** 111–31
[22] Johnson R W, Hultqvist A and Bent S F 2014 A brief review of atomic layer deposition: from fundamentals to applications *Mater. Today* **17** 236–46
[23] Park J H and Sudarshan T S 2001 Introduction to chemical vapour deposition (CVD) *Chemical Vapor Deposition* (ASM International) ch 1, pp 1–22
[24] Dobkin D and Zuraw M K 2003 Introduction *Principles of Chemical Vapor Deposition* (Springer Science & Business Media) ch 1, pp 1–8
[25] Keithley 2110 5.5 digit multimeter with dual display (available at: www.tek.com/en/products/keithley/digital-multimeter/2110-series)
[26] FLIR A6751 thermal camera (available at: www.flir.co.uk/)
[27] Wu R, Roberts P C E, Lyu S, Zheng F, Soutis C, Diver C, Zhou D, Li L and Deng Z 2021 Lightweight self-forming super-elastic mechanical metamaterials with adaptive stiffness *Adv. Funct. Mater.* **31** 2008252
[28] Choe J K, Yi J, Jang H, Won H, Lee S, Lee H, Jang Y, Song H and Kim J 2024 Digital mechanical metamaterial: encoding mechanical information with graphical stiffness pattern for adaptive soft machines *Adv. Mater.* **36** 2304302